Journal of Magnetics 17(2), 86-95 (2012) http://dx.doi.org/10.4283/JMAG.2012.17.2.086

Effects of Ni Addition on the Microstructures and Magnetic Properties of $Fe_{70-x}Pd_{30}Ni_x$ High-Temperature Ferromagnetic Shape Memory Alloys

Chien-Feng Lin* and Jin-Bin Yang

Department of Mechanical and Automatic Engineering, National Kaohsiung First University of Science and Technology, Kaohsiung, Taiwan, ROC

(Received 31 October 2011, Received in final form 29 April 2012, Accepted 3 May 2012)

This study investigated the effects of adding a third alloying element, Ni, to create $Fe_{70-x}Pd_{30}Ni_x$ (x = 2, 4, 6, 8 at.% Ni) ferromagnetic shape memory alloys (FSMAs). The Ni replaced a portion of the Fe. The $Fe_{70-x}Pd_{30}Ni_x$ alloys were homogenized through hot and cold forging to gain a ~38% reduction in thickness, next they were solution-treated (ST) with annealing recrystallization at 1100 °C for 8 h and quenched in ice brine, and then aged at 500 °C for 100 h. Investigation of the microstructures and magnetostriction indicated that the greater Ni amount in the $Fe_{70-x}Pd_{30}Ni_x$ alloys reduced saturation magnetostriction at room temperature (RT). It was also observed that it was more difficult to generate annealed recrystallization. However, with greater Ni addition into the $Fe_{70-x}Pd_{30}Ni_x$ (x = 6, 8 at.% Ni) alloys, the $L1_0$+$L1_m$ twin phase decomposition into stoichiometric $L1_0$+$L1_m$+α_{bct} structures was suppressed after the 500 °C/100 h aging treatment. The result was that the $Fe_{70-x}Pd_{30}Ni_x$ (x = 6, 8 at.% Ni) alloys maintained a high magnetostriction and magnetostrictive susceptibility ($\Delta\lambda_{\parallel}^{s}/\Delta H$) after the alloys were aged at 500 °C for 100 h. This magnetic property of the $Fe_{70-x}Pd_{30}Ni_x$ (x = 6, 8 at.% Ni) alloys make it suitable for application in a high temperature (T > 500 °C) and high frequency environments.

Keywords : $Fe_{70-x}Pd_{30}Ni_x$ alloys, SEM and TEM microstructures, x-ray diffraction, high-temperature magnetostriction

1. Introduction

Magnetic field control of high-temperature shape memory effects was recently suggested as a principle for the operation of a new type of actuator material. At present, a new class of high-temperature shape memory alloys (HTSMAs) has been widely investigated due to their ability to suppress transitions at high temperatures (exceeding 400 °C). This magnetic property makes HTSMAs suitable for actuation in the high-temperature environments commonly found in the aerospace, automotive and oil industries or in certain other devices [1-3]. The $Fe_{70}Pd_{30}$ alloys undergo successive martensitic phase transformations from FCC to FCT to BCT upon cooling [4]. The FCC-FCT transformation, which is thermoelastic and reversible, is suitable for actuator application. In contrast, the FCT-BCT transformation is irreversible, and it therefore destroys the ferromagnetic shape memory effect (FSME). However, the phase transformations of $Fe_{70-x}Pd_{30}Ni_x$ (x = 2, 4, 6, 8 at.% Ni) alloys are different from those of $Fe_{70}Pd_{30}$ alloy systems. In $Fe_{70-x}Pd_{30}Ni_x$ alloy systems, in a solution-treatment (ST) condition, the phases of the alloys mainly include martensitic $L1_0$+$L1_m$ twins [5]. After ST and aging treatment at 500 °C for 100 h, the addition of a small amount of Ni into the $Fe_{70-x}Pd_{30}Ni_x$ (x = 2, 4 at.% Ni) alloys causes the decomposition of the martensitic $L1_0$+$L1_m$ twin phase into stoichiometric $L1_0$+$L1_m$+α_{bct} structures, this does not occur with slightly larger Ni addition into the $Fe_{70-x}Pd_{30}Ni_x$ (x = 6, 8 at.% Ni) alloys. The reason is that with greater Ni amount in the $Fe_{70-x}Pd_{30}Ni_x$ (x = 6, 8 at.% Ni) alloys maintain a stable martensitic $L1_0$+$L1_m$ twin structure after the ST and aging at 500 °C for 100 h. The differences in Ni content of the $Fe_{70-x}Pd_{30}Ni_x$ alloys could be associated with the changes in martensitic transformation at high temperature (500 °C). In addition, in the $Fe_{70-x}Pd_{30}Ni_x$ (x = 2, 4, 6, 8 at.% Ni) alloy systems, the irreversible α_{bct} phase does not exist below room temperature. The α_{bct} phase found in the $Fe_{70-x}Pd_{30}Ni_x$ (x = 2, 4 at.% Ni) alloys after 500 °C/100 h aged treatment is due to $L1_0$+$L1_m$ phase decomposition. The present work aims to characterize the evolu-

*Corresponding author: Tel: +886 7 6011000
Fax: +886 7 6011069, e-mail: lin.lin3312@msa.hinet.net

tion of the martensitic transformation (MT) and magnetostriction changes produced by strain-forging with solution-treatment (ST) and aging at a high temperature of 500 °C for 100 h in polycrystalline $Fe_{70-x}Pd_{30}Ni_x$ (x = 2, 4, 6, 8 at.% Ni) alloys. In order to determine the thermal stability of the martensitic transformation (MT) and effects of aging on the magnetostriction, the compositions were varied in each alloy. Specifically, the Pd was maintained at close to 30 at.%, while the Ni and Fe contents were varied. The main results of the study reveal that with a larger addition of Ni into the $Fe_{70-x}Pd_{30}Ni_x$ (x = 6, 8 at.% Ni) alloys and subsequent thermo-mechanical treatments, the α_{bct} phases can be suppressed after the 500 °C/100 h aging treatment.

The motivation of this study arose from our previous investigation of $Fe_{66}Pd_{30}Ni_4$ (4 at.% Ni) alloys, in which we found that the $L1_0$+$L1_m$ martensitic twin phase decomposition into stoichiometric $L1_0$+$L1_m$+α_{bct} structures could be suppressed after the alloys were strain-forged, solution-treated, and aged at 400 °C for 100 h. Magnetostriction measurements of the alloys indicated that the samples aged at 400 °C/100 h had high magnetostrictive strains ($\lambda_{\parallel}^{s} = 62 \times 10^{-6}$; $\lambda_{\perp}^{s} = -11 \times 10^{-6}$) [5]. This good thermal stability is important for the practical application of high-temperature shape memory alloys (HTSMAs). However, when the $Fe_{66}Pd_{30}Ni_4$ alloys were aged at 500 °C for 100 h, the separation of $L1_0$+$L1_m$ martensitic twin phases into stoichiometric $L1_0$+$L1_m$+α_{bct} structures led to the destruction of the magnetostriction (i.e., damaged the ferromagnetic shape memory effect-FSME) [5]. Therefore, in this study, we investigated in detail the effects of varying the amount of Ni in $Fe_{70-x}Pd_{30}Ni_x$ (x = 2, 4, 6, 8 at.% Ni) alloys, and then strain-forged and solution treated samples before aging them at 500 °C for 100 h. The influence of high-temperature (500 °C/100 h) aging treatment on the microstructure, martensitic transformation behavior, *M-H* curve and magnetostriction was investigated in detail in order to evaluate their thermal stability for high-temperature applications.

2. Experimental Details

$Fe_{70-x}Pd_{30}Ni_x$ (x = 2, 4, 6, 8 at.% Ni) ferromagnetic shape memory alloys (FSMAs) were prepared by melting pure electrolytic iron (99.9%), pure palladium (99.95%), and pure nickel powder (99.95%) in an arc vacuum furnace under a controlled protective argon atmosphere. Samples were sliced from the cast ingot and sealed in an evacuated quartz capsule, where they were homogenized at 1050 °C for 70 hours, followed by quenching in ice-brine. After homogenization, the specimens were strain-forged to gain a ~38% reduction in thickness, polished, sealed in an evacuated quartz capsule again, and then solution treated (ST) and annealed for recrystallization at 1100 °C for 8 h, followed by quenching in ice brine. Aging of the samples was performed at 500 °C for 100 h. The microstructure observations with SEM were carried out with polished specimens etched in a solution of 60% HCl and 40% HNO_3 at a temperature of about 85 °C. A scanning electron microscope (SEM), model FEI QUANTA-400F SERIES, was used to examine the samples with the secondary electron (SE) image and energy dispersive spectroscopy (EDS) functions. Thin foils for TEM study were prepared by double jet electropolishing in a solution containing 75% acetic acid, 15% perchloric acid, and 10% methanol in a temperature range of –7 °C~10 °C using a current density of 2 A/cm^2 to 4 A/cm^2. Transmission electron microscopy (TEM), with a double tilt stage, was performed in an analytical type, high resolution electron microscope (Hitachi HF-2000) with the field emission gun operated at 200 kV and a JEM-2100F TEM operated at 200 kV, respectively. The x-ray diffraction (XRD) patterns were detected at room temperature using an x-ray diffractometer (Siemens D5000 Karlsruhe) with Cu-K_α radiation, and diffraction angles were in the 2θ ranges from 35° to 140°. The hysteresis loop measurements were performed with a superconducting quantum interference device (SQUID) magnetometer. The magnetization versus magnetic field (*M-H*) curves for the samples were measured at room temperature (300 K) and low temperature (100 K) with a maximum applied field of 10000 Oe. The magnetization measurements were performed on a specimen with dimensions of 5 mm (length) × 1 mm (width) × 1 mm (thickness). The magnetostriction measurements were taken with a strain gauge and Vishay Micro-Measurements Model P3 strain indicator and recorder. A sample with dimensions of 15 mm (length) × 5 mm (width) × 1 mm (thickness) was used for the magnetostriction measurements. A FLA-2-11-A515411 type strain gauge, purchased from TML (Tokyo Sokki Kenkyujo Co. Ltd.), was used. The gauge was glued to the sample along its longitude with an M-Bond 200 Adhesive Kit. To cure the glue, both the gauge and the specimen were kept at RT for 2 days. Then the magnetostrictive strains were measured.

3. Results and Discussion

3.1. Microstructure investigations

Figures 1(a)-(d) show the SEM micrographs of the $Fe_{70-x}Pd_{30}Ni_x$ (x = 2, 4, 6, 8 at.% Ni) alloys homogenized and strain-forged to gain a ~38% reduction in thickness, annealed for recrystallization (i.e., ST) at 1100 °C for 8 h,

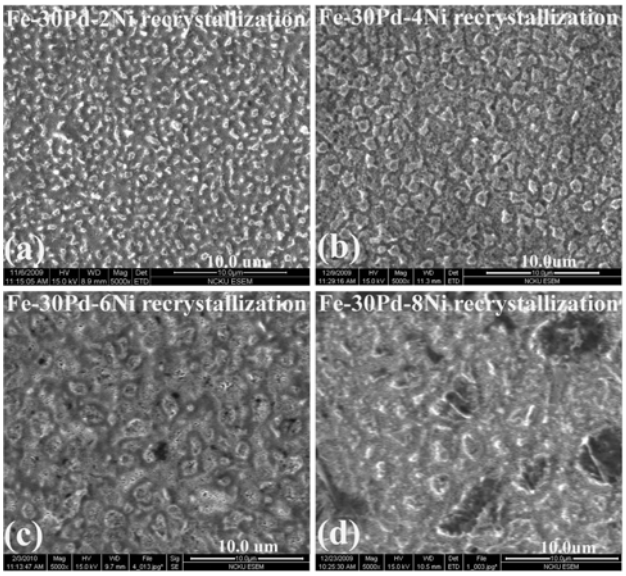

Fig. 1. (a)-(d) SEM images of the $Fe_{70-x}Pd_{30}Ni_x$ (x = 2, 4, 6, 8 at.% Ni) alloys strain-forged to gain a ~38% reduction in thickness, solution-treated (ST), and annealed for recrystallization at 1100 °C for 8 h.

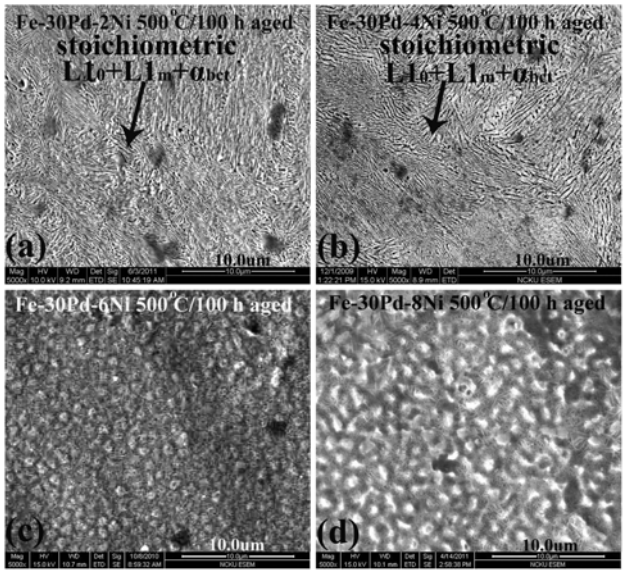

Fig. 2. (a)-(d) SEM images of the $Fe_{70-x}Pd_{30}Ni_x$ (x = 2, 4, 6, 8 at.% Ni) alloys strain-forged to gain a ~38% reduction in thickness, solution-treated, and annealed for recrystallization at 1100 °C for 8 h, then aged at 500 °C for 100 h.

and quenched in ice brine. The fine grain (0.2-2 μm) microstructures developed by recrystallization are clearly present. By careful analysis of the SEM microstructures and magnetostriction data (Fig. 11), it is found that after recrystallization, the strain-forged $Fe_{68}Pd_{30}Ni_2$ (2 at.% Ni) alloys have fine grains with high magnetostrictive strains ($\lambda_{\parallel}^{s} = 88 \times 10^{-6}$; $\lambda_{\perp}^{s} = -26 \times 10^{-6}$), while the strain-forged $Fe_{62}Pd_{30}Ni_8$ (8 at.% Ni) alloys, after recrystallization, have coarse grains with low magnetostrictive strains ($\lambda_{\parallel}^{s} = 57 \times 10^{-6}$; $\lambda_{\perp}^{s} = -15 \times 10^{-6}$). The SEM image analysis and magnetostriction measurement (Fig. 11) results indicate that adding more Ni into the $Fe_{70-x}Pd_{30}Ni_x$ alloys limits the generation of a fine grain structure when the alloys are strain-forged and then annealed for recrystallization. This results in high Ni-content alloys with a coarse grain structure and low magnetostriction at room temperature. In addition, our experimental results also demonstrate that grain size reduction through strain-forging and annealing for recrystallization improves not only the strength and toughness but also the magnetostriction and magnetostrictive susceptibility ($\Delta\lambda_{\parallel}^{s}/\Delta H$) of the $Fe_{70-x}Pd_{30}Ni_x$ (x = 2, 4, 6, 8 at.% Ni) alloys.

Shown in Figs. 2(a)-(b) are SEM microstructures of the $Fe_{68}Pd_{30}Ni_2$ (2 at.% Ni) and $Fe_{66}Pd_{30}Ni_4$ (4 at.% Ni) alloys homogenized through strain forging and recrystallization annealing (i.e., ST) at 1100 °C for 8 h, and then aged at 500 °C for 100 h. The decomposition of the $L1_0$+$L1_m$ twin phase into stoichiometric $L1_0$+$L1_m$+α_{bct} structures, indicated by the arrow, is apparent in both 500 °C/100 h aged samples. The lamellar stoichiometric $L1_0$+$L1_m$+α_{bct} structures are similar to pearlite, but x-ray diffraction pattern analysis confirmed that these lamellar structures contained $L1_0$+$L1_m$+α_{bct} phases, as shown in Figs. 7(a)-(b). Magnetostriction measurements indicate that these $L1_0$+$L1_m$+α_{bct} structures have low magnetostrictive strains, as illustrated in Fig. 12. Figures 2(c)-(d) are SEM images of the $Fe_{64}Pd_{30}Ni_6$ (6 at.% Ni) and $Fe_{62}Pd_{30}Ni_8$ (8 at.% Ni) alloys homogenized through strain-forging and recrystallization annealing at 1100 °C for 8 h and then aged at 500 °C for 100 h. The decomposition of the $L1_0$+$L1_m$ twin phase into stoichiometric $L1_0$+$L1_m$+α_{bct} structures is not evident in these SEM images. X-ray diffraction patterns also indicate that the $Fe_{70-x}Pd_{30}Ni_x$ alloy with Ni = 6 (8 at.%), after strain forging, ST and aging at 500 °C for 100 h, can suppress the $L1_0$+$L1_m$ twin phase separation into stoichiometric $L1_0$+$L1_m$+α_{bct} structures, as shown in Figs. 7(c)-(d). As a result, the $Fe_{64}Pd_{30}Ni_6$ (6 at.% Ni) and $Fe_{62}Pd_{30}Ni_8$ (8 at.% Ni) alloys after strain forging, ST, and aging at 500 °C for 100 h maintain high magnetostrictive strains, as demonstrated in Fig. 12. This magnetic property of the $Fe_{70-x}Pd_{30}Ni_x$ (x = 6, 8 at.% Ni) alloys make it suitable for application in high temperature (T > 500 °C) and high frequency environments.

To confirm that the separated lamellar structures were stoichiometric, higher magnification SEM images of the $Fe_{66}Pd_{30}Ni_4$ (4 at.% Ni) alloys strain-forged to gain a ~38% reduction, ST, and aged at 400 °C/100 h and 500 °C /100 h are shown in Figs. 3(a)-(d). Shown in Fig. 3(a) is

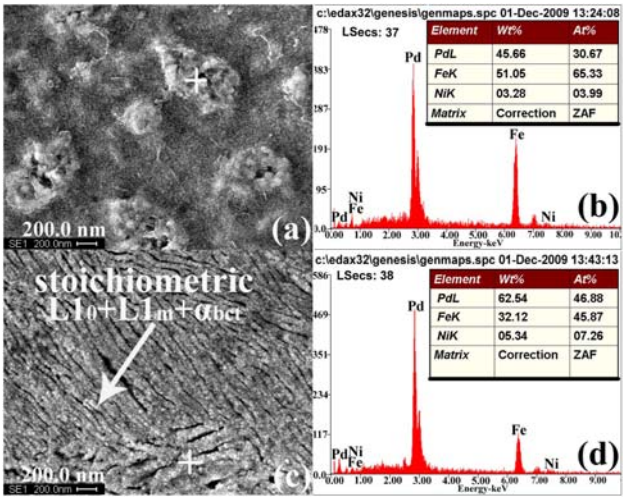

Fig. 3. (a)-(d) (Color online) (a) SEM image of the $Fe_{66}Pd_{30}Ni_4$ (4 at.% Ni) alloys strain-forged to gain a ~38%, ST, and aged at 400 °C for 100 h, (b) EDS taken from (a) marked with +, (c) SEM micrograph of the same strain-forged alloys ST and aged at 500 °C for 100 h, (d) EDS taken from (c) marked with +, showing that the stoichiometric $L1_0$ ordered structure takes place at a composition around 1:1 of Fe and Pd.

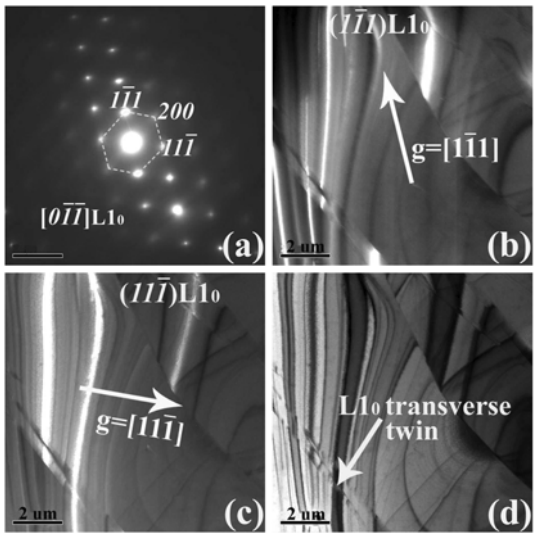

Fig. 4. TEM images of the $Fe_{66}Pd_{30}Ni_4$ (4 at.% Ni) alloys strain forged to gain a ~38% thickness reduction and solution-treated (ST) at 1100 °C for 8 h: (a) SADP of zone axis $[0\ \bar{1}\ \bar{1}]_{L10}$ (*hkl* denotes tetragonal $L1_0$ reflection), (b) DF image of $(1\ \bar{1}\ 1)_{L10}$ reflection corresponding to (a), (c) DF image of $(1\ 1\ \bar{1})_{L10}$ reflection corresponding to (a), and (d) BF image, the transverse twin indicated by arrow.

the strain-forged $Fe_{66}Pd_{30}Ni_4$ alloy ST and aged at 400 °C for 100 h, in which the $L1_0$+$L1_m$ phase separation into a stoichiometric $L1_0$+$L1_m$+α_{bct} lamellar structure was suppressed. Figure 3(b) is the energy dispersive spectroscopy (EDS) spectra taken from Fig. 3(a), marked with +, it reveals a chemical composition content of about Fe(65.33)-Pd(30.67)-Ni(3.99) (at.%). This indicates a non-stoichiometric $L1_0$ structure, which has optimal magnetostrictive strains ($\lambda_{\parallel}^{s} = 62 \times 10^{-6}$; $\lambda_{\perp}^{s} = -11 \times 10^{-6}$) [5]. Figure 3(c) is a higher magnification SEM micrograph of the same strain-forged alloys ST and aged at 500 °C for 100 h. This image shows the decomposition of the $L1_0$+$L1_m$ phases into the stoichiometric $L1_0$+$L1_m$+α_{bct} structures, indicated by the arrow. Figure 3(d) presents the EDS spectra taken from the separated stoichiometric $L1_0$+$L1_m$+α_{bct} regions (in Fig. 3(c)) marked with +, it reveals a chemical composition content of Fe(45.87)-Pd(46.88)-Ni(7.26) (at.%). This content is consistent with a typical stoichiometric $L1_0$ structure with an Fe content of about (45.87 at.%) and Pd content of about (46.88 at.%), in which the stoichiometric $L1_0$ ordering phase takes place at a composition with a ratio of around 1:1 of Fe and Pd, forming a stable structure in the vicinity of the equiatomic composition. Due to symmetry constraints imposed by the layered $L1_0$ order, some parts of the twin boundaries connecting different stoichiometric $L1_0$ variants are immobilized. Therefore, the separated stoichiometric $L1_0$+$L1_m$+α_{bct} structures lead to a decrease in the optimal magnetostriction ($\lambda_{\parallel}^{s} = 22 \times 10^{-6}$; $\lambda_{\perp}^{s} = -7 \times 10^{-6}$), as illustrated in Fig. 12.

The TEM micrographs of the $Fe_{66}Pd_{30}Ni_4$ (4 at.% Ni) alloys strain forged to gain a ~38% reduction in thickness and thermally ST at 1100 °C for 8 h are shown in Figs. 4(a)-(d). Figure 4(a) shows a selected area diffraction pattern (SADP) with zone axis $[0\ \bar{1}\ \bar{1}]_{L10}$ (*hkl* denotes a tetragonal $L1_0$ structure and an ordered $L1_0$ martensitic structure with lattice parameters of a = 3.807 Å, c = 3.657 Å, and c/a = 0.96). Figure 4(b) is a dark field (DF) image using the $(1\ \bar{1}\ 1)_{L10}$ reflection corresponding to Fig. 4(a). The bright contrast shows the martensitic $L1_0$ twin structures, which contribute magnetostriction in the alloys that may be useful in actuator applications. A DF image using the $(1\ 1\ \bar{1})_{L10}$ reflection corresponding to Fig. 4(a) is shown in Fig. 4(c), in which the bright contrast also represents martensitic $L1_0$ twin structures. The above-mentioned $L1_0$ martensitic twins provide a lattice invariant shear for maintaining an invariant habit plane [6-8]; therefore, they are expected to contribute to higher magnetostriction in the alloys for use in magneto-mechanical applications (such as for microactuators or springs). Figure 4(d) is a bright field (BF) image, with the transverse twin indicated by an arrow. We took many TEM micrographs of the strain-forged $Fe_{70-x}Pd_{30}Ni_x$ samples, and of not strain-forged specimens with the same annealing treatment. We discovered that the trans-

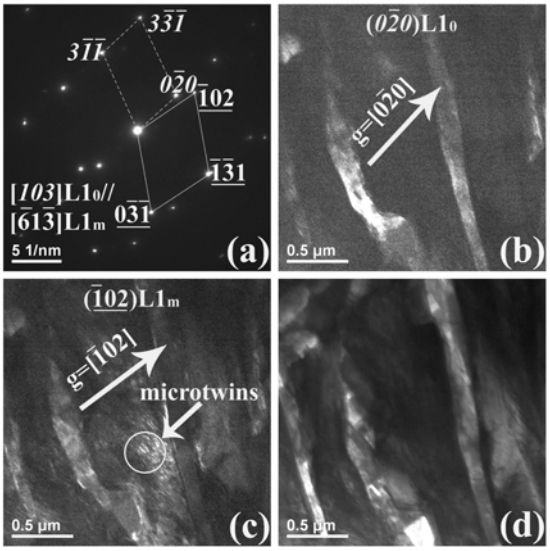

Fig. 5. TEM images of the $Fe_{64}Pd_{30}Ni_6$ (6 at.% Ni) alloys strain forged to gain a ~38% thickness reduction, solution-treated (ST) at 1100 °C for 8 h, and aged at 500 °C for 100 h: (a) SADP of zone axis $[103]_{L10}//[\bar{6}\ 1\ \bar{3}]_{L1m}$ (*hkl* denotes a tetragonal stoichiometric $L1_0$ structure; hkl denotes an $L1_m$ monoclinic martensitic phase), (b) DF image of $(0\ \bar{2}\ 0)_{L10}$ reflection corresponding to (a), (c) DF image of $(\underline{102})_{L1m}$ reflection corresponding to (a), and (d) BF image.

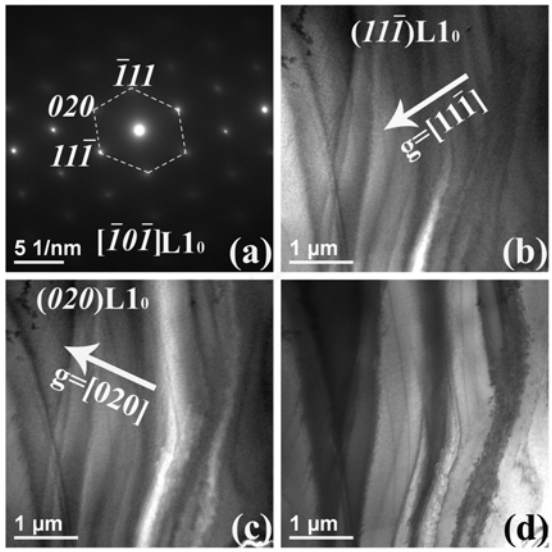

Fig. 6. TEM images of the $Fe_{62}Pd_{30}Ni_8$ (8 at.% Ni) alloys strain forged to gain a ~38% thickness reduction and solution-treated (ST) at 1100 °C for 8 h: (a) SADP of zone axis $[\bar{1}\ 0\ \bar{1}]_{L10}$ (*hkl* denotes a tetragonal $L1_0$ reflection), (b) DF image of $(1\ 1\ \bar{1})_{L10}$ reflection corresponding to (a), (c) DF image of $(020)_{L10}$ reflection corresponding to (a), and (d) BF image.

verse twins could not be found in the not strain-forged samples. In addition, from magnetostriction measurements, we found that the magnetostrictive strains of the $Fe_{70-x}Pd_{30}Ni_x$ alloys strain-forged and annealed for recrystallization were higher than those of not strain-forged alloys with the same annealing treatment. Whether the higher magnetostrictive strains can be ascribed to the transverse twins or not remains unclear.

Figures 5(a)-(d) are TEM micrographs of $Fe_{64}Pd_{30}Ni_6$ (6 at.% Ni) alloys strain forged to gain a ~38% thickness reduction, thermally ST at 1100 °C for 8 h, and aged at 500 °C for 100 h. Figure 5(a) is an SADP with zone axis $[103]_{L10}//[\bar{6}\ 1\ \bar{3}]_{L1m}$ (*hkl* denotes a tetragonal stoichiometric $L1_0$ structure with lattice parameters of a = 3.813 Å, c = 3.636 Å, and c/a = 0.954; hkl denotes a monoclinic $L1_m$ phase with lattice parameters of a = 3.140 Å, b = 3.813 Å, c = 3.110 Å, and $\beta = 92.261°$). A dark field (DF) image using the stoichiometric $(0\ \bar{2}\ 0)_{L10}$ reflection corresponding to Fig. 5(a) is shown in Fig. 5(b), in which the bright contrast represents the phase separated stoichiometric $L1_0$ structure, which belongs to a second order phase with a primitive crystal structure. A dark field image taken using $(\underline{\bar{1}02})_{L1m}$ reflection corresponding to Fig. 5(a) is shown in Fig. 5(c), in which the bright contrast represents the monoclinic $L1_m$ phase. The DF image of Fig. 5(c) reveals that the $L1_m$ monoclinic phases are comprised of periodic alternating microtwins, as indicated with a circle. A comparison of Figs. 5(b) and 5(c) reveals distinct differences in the microstructures of the stoichiometric $L1_0$ structure and the monoclinic $L1_m$ phase. Analysis of the microstructures (Figs. 5(b) and 5(c)) confirms unambiguously the existence of two phases (i.e., the stoichiometric $L1_0$ structure and $L1_m$ phase) in the phase decomposition morphology. Figure 5(d) is a corresponding typical BF image of the phase decomposition morphology of the stoichiometric $L1_0$+$L1_m$ structures.

Figures 6(a)-(d) show a series of TEM micrographs of $Fe_{62}Pd_{30}Ni_8$ (8 at.% Ni) alloys strain forged to gain a ~38% thickness reduction and thermally ST at 1100 °C for 8 h. Figure 6(a) is a selected area diffraction pattern (SADP) with zone axis $[\bar{1}\ 0\ \bar{1}]_{L10}$ (*hkl* denotes a tetragonal $L1_0$ structure and an ordered $L1_0$ martensitic structure with lattice parameters of a = 3.808 Å, c = 3.633 Å, and c/a = 0.954). Figure 6(b) is a dark field (DF) image using the $(1\ 1\ \bar{1})_{L10}$ reflection corresponding to Fig. 6(a). The bright contrast shows the martensitic $L1_0$ twin structures, which contribute to magnetostriction in the alloys that may be useful in high-temperature actuator application. A DF image using the $(020)_{L10}$ reflection corresponding to Fig. 6(a) is shown in Fig. 6(c), in which the bright contrast also represents the martensitic $L1_0$ twin structures. These martensitic $L1_0$ twins provide a lattice invariant shear for maintaining an invariant habit plane; therefore, they are expected to contribute to the ferromagnetic shape

memory effect (FSME) in the alloys for use in high temperature magneto-mechanical applications (such as for microactuators or springs). Figure 6(d) is a bright field (BF) image. A comparison of Fig. 6 with Fig. 4 demonstrates that different amounts of Ni content in the $Fe_{70-x}Pd_{30}Ni_x$ alloys generate distinct differences in the microstructures of the martensitic $L1_0$ twin phase.

3.2. X-ray diffraction pattern analysis

Figures 7(a)-(d) represent a series of x-ray diffraction (XRD) patterns of the $Fe_{70-x}Pd_{30}Ni_x$ (x = 2, 4, 6, 8 at.% Ni) alloys strain-forged to gain a ~38% thickness reduction, ST at 1100 °C for 8 h, and aged at 500 °C for 100 h. Shown in Figs. 7(a)-(b) are the XRD patterns of the $Fe_{68}Pd_{30}Ni_2$ (2 at.% Ni) and $Fe_{66}Pd_{30}Ni_4$ alloys ST aged at 500 °C for 100 h, in which the reflections are comprised of two phases ($L1_0$+$L1_m$), with the main diffraction peaks being the reflection of $(111)_{L10}$ and $(101)_{L1m}$. These XRD patterns also show that the $(101)_{\alpha bct}$ peak appears at a diffraction angle of $2\theta = 44.60°$ in Fig. 7(a), and at $2\theta = 44.52°$ in Fig. 7(b), along with many new diffraction peaks revealed in the diffraction patterns. These datum demonstrate the decomposition of the $L1_0$+$L1_m$ twin phase into stoichiometric $L1_0$+$L1_m$+α_{bct} structures in these 500 °C/100 h aged $Fe_{70-x}Pd_{30}Ni_x$ (x = 2, 4 at.% Ni) alloys, which lead to low magnetostriction, as shown in Fig. 12.

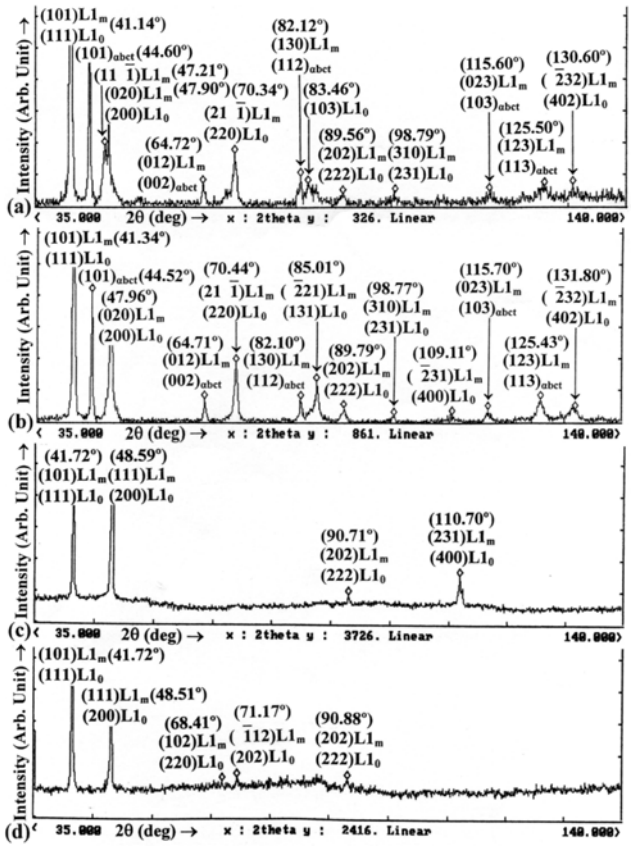

Fig. 7. X-ray diffraction (XRD) patterns: (a) $Fe_{68}Pd_{30}Ni_2$ (2 at.% Ni), (b) $Fe_{66}Pd_{30}Ni_4$, (c) $Fe_{64}Pd_{30}Ni_6$, and (d) $Fe_{62}Pd_{30}Ni_8$ alloys strain-forged to gain a ~38% reduction in thickness, solution treated (ST) at 1100 °C for 8 h, quenched in ice brine, and then aged at 500 °C for 100 h (41.14° denotes diffraction angle $2\theta = 41.14°$).

The XRD patterns of the strain-forged $Fe_{64}Pd_{30}Ni_6$ (6 at.% Ni) and $Fe_{62}Pd_{30}Ni_8$ alloys after ST at 1100 °C for 8 h and aging at 500 °C for 100 h are shown in Figs. 7(c) and 7(d). An analysis of Figs. 7(c) and 7(d) reveals no $(101)_{\alpha bct}$ peaks in the x-ray diffraction patterns; nor can we observe any new diffraction peaks in the diffraction patterns. These phenomena indicate that the decomposition of the $L1_0$+$L1_m$ twin phases into stoichiometric $L1_0$+$L1_m$+α_{bct} structures was suppressed after the strain-forging of the $Fe_{70-x}Pd_{30}Ni_x$ (x = 6, 8 at.% Ni) alloys that were ST and aged at 500 °C for 100 h, as a result they maintain higher magnetostriction and magnetostrictive susceptibility ($\Delta\lambda_{\|}^{s}/\Delta H$), as shown in Fig. 12. The XRD results demonstrate that with a greater addition of Ni in $Fe_{70-x}Pd_{30}Ni_x$ (x = 6, 8 at.% Ni) alloys, the separation of $L1_0$+$L1_m$ twin phase into stoichiometric $L1_0$+$L1_m$+α_{bct} structures can be suppressed after aging treatment at 500 °C/100 h, and the ferromagnetic shape memory effect (FSME) at high temperature is improved. These magnetic properties of the $Fe_{70-x}Pd_{30}Ni_x$ (x = 6, 8 at.% Ni) alloys make them suitable for application in high temperature ($T > 500$ °C) and high frequency environments [9]. Stable actuation at high frequencies has recently been required in the aerospace, automotive, and oil industries. However, in a high frequency environment, the actuator temperature sometimes approaches a high-temperature. Most actuator materials cannot work for a long time in high-temperature environments owing to phase decomposition. However, the $Fe_{70-x}Pd_{30}Ni_x$ FSM alloys have a high saturation magnetization, high magnetocrystalline anisotropy energy constant (K_u), high permeability and high magnetostrictive susceptibility ($\Delta\lambda_{\|}^{s}/\Delta H$). The relationship between the strain derivative and the sensitivity of magnetization to applied stress can be expressed as: $(\Delta\lambda_{\|}^{s}/\Delta H)_{\sigma} = \mu_0 \times (\Delta B/\Delta\sigma)_H$ (where λ is the magnetostrictive strain and H is the magnetic field; μ_0 is the permeability of free space, B is the magnetic flux density, and σ is the stress). Thus, high magnetostrictive susceptibility is indicative of promising characteristics for a magnetoelastic actuator material such as $Fe_{70-x}Pd_{30}Ni_x$ FSM alloys. In addition, the most important experimental finding is that the $Fe_{64}Pd_{30}Ni_6$ and $Fe_{62}Pd_{30}Ni_8$ FSM alloys do not generate phase separation after aging at 500 °C/100 h. Therefore, the alloys should be suitable for application in a high frequency (high

temperature) environment.

3.3. Magnetic properties

The mass magnetization (M) vs. magnetic field (H) curves of the strain-forged to gain a ~38% thickness reduction $Fe_{66}Pd_{30}Ni_4$ (4 at.% Ni) alloys ST and aged at 500 °C for 100 h, were measured at RT (300 K) and low temperature (100 K). The results are shown in Fig. 8, where $H_{\|}$ denotes the magnetic applied field parallel to the sample's longitude, and $H_{\perp}$ denotes the magnetic applied field normal to the sample's longitude (i.e., out of plane: the perpendicular field applied to the sample's cross section region was 5 mm in length). As shown in Fig. 8, the M-H curves were magnetically hard, with a coercivity H_c = 500-600 Oe for the sample after ST and aging at 500 °C for 100 h. Also, at RT (300 K), the saturation magnetization (M_s) of the magnetic moment per unit mass $M_{s(300\ K)\|}$ = 137.13 (emu/g) for $H_{a\|}$ = 3 kOe and $M_{s(300\ K)\perp}$ = 124.87 (emu/g) for $H_{a\perp}$ = 9 kOe, while at low temperature (100 K) $M_{s(100\ K)\|}$ = 140.90 (emu/g) for $H_{a\|}$ = 3 kOe and $M_{s(100\ K)\perp}$ = 127.13 (emu/g) for $H_{a\perp}$ = 9 kOe. The value of the magnetocrystalline anisotropy energy constant (K_u) from equation $K_u = M_s \times H_a \times \rho/2$ (where M_s: saturation magnetization, H_a: anisotropy field, with theoretical density ρ = 9.350 (g/cm^3)) was obtained as follows: $K_{u(300\ K)\|} = 1.92 \times 10^6$ (ergs/cm^3); $K_{u(300\ K)\perp} = 5.25 \times 10^6$ (ergs/cm^3), and $K_{u(100\ K)\|} = 1.98 \times 10^6$ (ergs/cm^3); $K_{u(100\ K)\perp} = 5.35 \times 10^6$ (ergs/cm^3), respectively [10].

The M-H curves, measured at RT (300 K) and low temperature (100 K), of the strain-forged $Fe_{64}Pd_{30}Ni_6$ (6 at.% Ni) alloys ST and aged at 500 °C for 100 h are shown in Fig. 9, in which the M-H curves are magnetically soft, with a small coercivity H_c = 50 Oe. The hysteresis loops at RT (300 K) reveal that the saturation magnetization (M_s) of the magnetic moment per unit mass $M_{s(300\ K)\|}$ = 145.22 (emu/g) for $H_{a\|}$ = 3 kOe; $M_{s(300\ K)\perp}$ = 141.67 (emu/g) for $H_{a\perp}$ = 8.5 kOe; and at low temperature (100 K), the $M_{s(100\ K)\|}$ = 153.85 (emu/g) for $H_{a\|}$ = 3 kOe; $M_{s(100\ K)\perp}$ = 150.11 (emu/g) for $H_{a\perp}$ = 8.5 kOe, respectively. The value of the magnetocrystalline anisotropy energy constant (K_u) from equation $K_u = M_s \times H_a \times \rho/2$ (where M_s: saturation magnetization, H_a: anisotropy field, with theoretical density ρ = 9.3697 (g/cm^3)) was obtained as follows: $K_{u(300\ K)\|} = 2.04 \times 10^6$ (ergs/cm^3); $K_{u(300\ K)\perp} = 5.64 \times 10^6$ (ergs/cm^3), and $K_{u(100\ K)\|} = 2.16 \times 10^6$ (ergs/cm^3); $K_{u(100\ K)\perp} = 5.98 \times 10^6$ (ergs/cm^3), respectively. From the hysteresis loop data (Figs. 8-9), it was found that the magnetic properties of both $Fe_{70-x}Pd_{30}Ni_x$ (x = 4, 6 at.% Ni) alloys after aging at 500 °C for 100 h, tested at lower temperature (100 K), had a higher saturated magnetization (M_s) as well as a higher magnetocrystalline anisotropy energy constant (K_u). This phenomenon is ascribed to the martensitic transformation from the mixed $L1_0$+$L1_m$ phases to a single $L1_0$ structure when the alloys were tested at lower temperature (100 K). Comparing Fig. 8 with Fig. 9, it was also found that after ST and aging at 500 °C for 100 h, the $Fe_{66}Pd_{30}Ni_4$ (4 at.% Ni) alloys increased in coercivity and underwent a decrease in saturation magnetization. This was due to the low Ni content of the $Fe_{66}Pd_{30}Ni_4$ (4 at.% Ni) alloys; during aging at 500 °C for 100 h, partial $L1_0$+$L1_m$ twin phase decomposition into the stoichiometric $L1_0$+$L1_m$+α_{bct} structure occurred, while in high Ni-content $Fe_{64}Pd_{30}Ni_6$ (6 at.% Ni) alloys, it did not. The change in magnetic properties is related to the $L1_0$+$L1_m$ martensitic

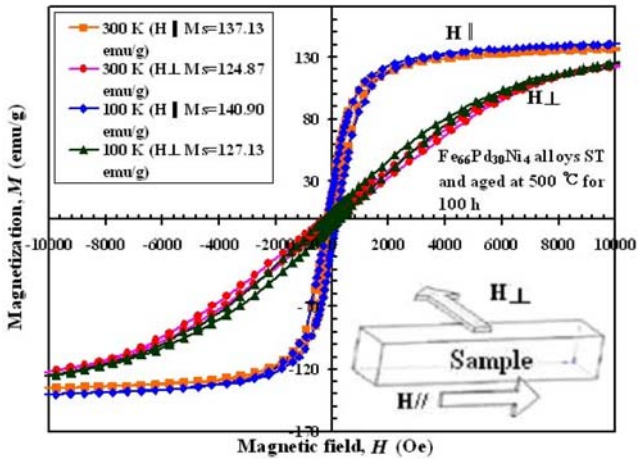

Fig. 8. (Color online) Magnetization (M) vs. magnetic field (H) curves measured at temperatures of 300 K (RT) and 100 K for the $Fe_{66}Pd_{30}Ni_4$ alloys strain-forged to gain a ~38% reduction in thickness, ST, and aged at 500 °C for 100 h.

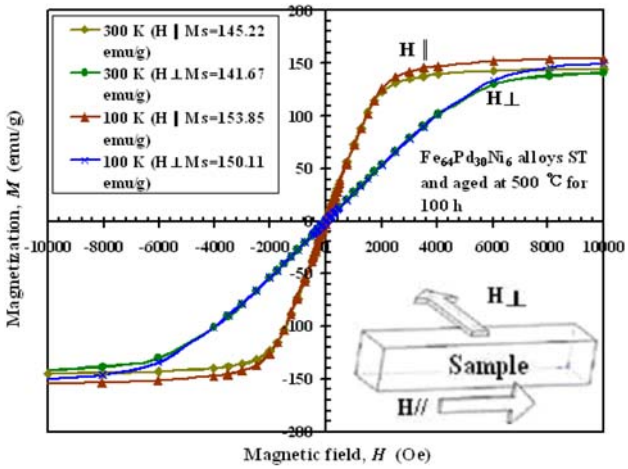

Fig. 9. (Color online) Magnetization (M) vs. magnetic field (H) curves measured at temperatures of 300 K (RT) and 100 K for the $Fe_{64}Pd_{30}Ni_6$ alloys strain-forged to gain a ~38% reduction in thickness, ST, and aged at 500 °C for 100 h.

Table 1. Summary of the magnetic properties (M_s: saturation magnetization and K_u: magnetocrystalline anisotropy energy constant) measured at 300 K (RT) and 100 K of $Fe_{70-x}Pd_{30}Ni_x$ (x = 4, 6 at.% Ni) alloys ST and then aged at 500 °C for 100 h.

ST and 500 °C/100 h aged alloys	300 K	100 K
$Fe_{66}Pd_{30}Ni_4$ alloys (theoretical density ρ = 9.350 (g/cm^3))	$M_{s(300\ K)\parallel}$ = 137.13 (emu/g) $M_{s(300\ K)\perp}$ = 124.87 (emu/g) **$K_{u(300\ K)\parallel}$ = 1.92 × 10^6 (ergs/cm^3)** **$K_{u(300\ K)\perp}$ = 5.25 × 10^6 (ergs/cm^3)**	$M_{s(100\ K)\parallel}$ = 140.90 (emu/g) $M_{s(100\ K)\perp}$ = 127.13 (emu/g) **$K_{u(100\ K)\parallel}$ = 1.98 × 10^6 (ergs/cm^3)** **$K_{u(100\ K)\perp}$ = 5.35 × 10^6 (ergs/cm^3)**
$Fe_{64}Pd_{30}Ni_6$ alloys (theoretical density ρ = 9.3697 (g/cm^3))	$M_{s(300\ K)\parallel}$ = 145.22 (emu/g) $M_{s(300\ K)\perp}$ = 141.67 (emu/g) **$K_{u(300\ K)\parallel}$ = 2.04 × 10^6 (ergs/cm^3)** **$K_{u(300\ K)\perp}$ = 5.64 × 10^6 (ergs/cm^3)**	$M_{s(100\ K)\parallel}$ = 153.85 (emu/g) $M_{s(100\ K)\perp}$ = 150.11 (emu/g) **$K_{u(100\ K)\parallel}$ = 2.16 × 10^6 (ergs/cm^3)** **$K_{u(100\ K)\perp}$ = 5.98 × 10^6 (ergs/cm^3)**

twin phase decomposition, confirmed here by the SQUID magnetic property test, in association with microstructure observation, as confirmed by SEM and x-ray diffraction, shown in Figs. 2(b)-(c) and Figs. 7(b)-(c). A summary of the magnetic properties, measured at 300 K (RT) and 100 K, of $Fe_{70-x}Pd_{30}Ni_x$ (x = 4, 6 at.% Ni) alloys ST and then aged at 500 °C for 100 h are listed in Table 1.

Figure 10 shows the saturation magnetostriction (λ_s) vs. magnetic field (H) curves, or λ_s–H curves, measured at room temperature (RT), of the as received $Fe_{70-x}Pd_{30}Ni_x$ (x = 2, 4, 6, 8 at.% Ni) alloys. The saturation magnetostriction λ_s is evaluated as $\lambda_s = (2/3)\times[(\lambda_\parallel)–(\lambda_\perp)]$, where $\lambda_\parallel$ ($\lambda_\perp$) is the magnetostriction in the longitudinal direction with a magnetic field parallel (perpendicular) to the sample's longitude. It can be seen in Fig. 10 that the saturation magnetostriction of the as received $Fe_{68}Pd_{30}Ni_2$ (2 at.% Ni) alloys (48×10^{-6}) is larger than that of the as received $Fe_{62}Pd_{30}Ni_8$ (8 at.% Ni) alloys (36.7×10^{-6}). In Fig. 10, the saturation magnetostriction of the as received $Fe_{70-x}Pd_{30}Ni_x$ (x = 2, 4, 6, 8 at.% Ni) alloys reveals that greater Ni addition in the alloys results in less saturation magnetostriction.

Figure 11 shows the magnetostrictive strains of the $Fe_{70-x}Pd_{30}Ni_x$ (x = 2, 4, 6, 8 at.% Ni) alloys homogenized and then strain-forged to gain a 38% reduction in thickness, solution treated (ST), and annealed at 1100 °C for 8 h for recrystallization, followed by quenching in ice brine. λ denotes $(\Delta L/L)_\parallel$ with a magnetic applied field parallel to the sample's longitude, and $\lambda_\perp$ denotes $(\Delta L/L)_\perp$ with a magnetic applied field normal to the sample's longitude (i.e., the direction of the perpendicular field: along the sample's width (5mm)). Two typical $\lambda_\parallel$ and $\lambda_\perp$ curves as a function of magnetic applied field can be seen in Fig. 11. The optimal magnetostriction $\lambda_\parallel^s$ and $\lambda_\perp^s$ with magneto-

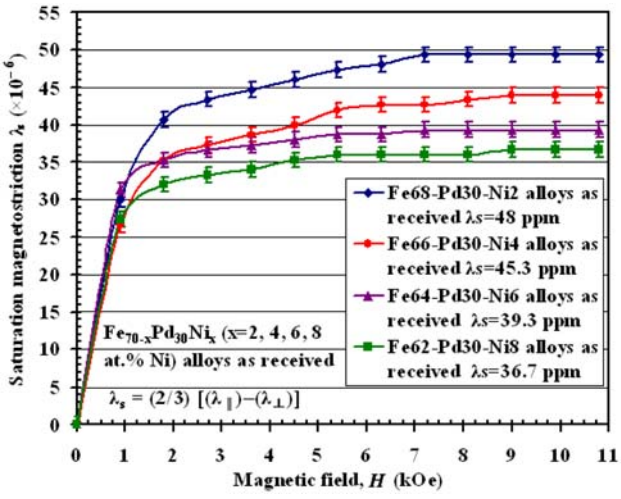

Fig. 10. (Color online) The linear saturation magnetostriction λ_s ($\times 10^{-6}$) vs. magnetic field (H) λ_s–H curves measured at room temperature of the as received $Fe_{70-x}Pd_{30}Ni_x$ (x = 2, 4, 6, 8 at.% Ni) alloys.

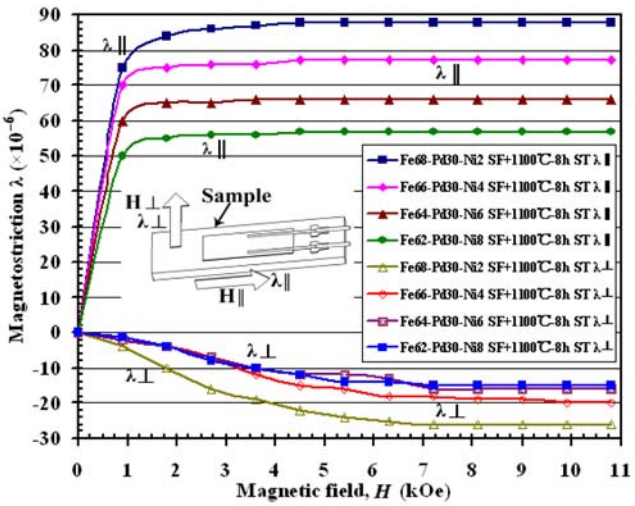

Fig. 11. (Color online) The linear magnetostriction ($\times 10^{-6}$) at RT (300 K) in parallel ($\lambda_\parallel$) and normal ($\lambda_\perp$) applied field (H (kOe)) to the sample's longitude for the $Fe_{70-x}Pd_{30}Ni_x$ (x = 2, 4, 6, 8 at.% Ni) alloys strain-forged (SF) to gain a ~38% reduction in thickness and then solution-treated (ST) and recrystallization annealed at 1100 °C for 8 h.

strictive susceptibility ($\Delta\lambda_{\parallel}^{s}/\Delta H$) are plotted as a function of applied field (H) at RT (300 K) for the various Ni-content samples, indicating the following: $\lambda_{\parallel}^{s} = 88 \times 10^{-6}$, $\lambda_{\perp}^{s} = -26 \times 10^{-6}$ for $Fe_{68}Pd_{30}Ni_2$ (2 at.% Ni) alloys; $\lambda_{\parallel}^{s} = 77 \times 10^{-6}$, $\lambda_{\perp}^{s} = -20 \times 10^{-6}$ for $Fe_{66}Pd_{30}Ni_4$ alloys; $\lambda_{\parallel}^{s} = 66 \times 10^{-6}$, $\lambda_{\perp}^{s} = -16 \times 10^{-6}$ for $Fe_{64}Pd_{30}Ni_6$ alloys; and $\lambda_{\parallel}^{s} = 57 \times 10^{-6}$, $\lambda_{\perp}^{s} = -15 \times 10^{-6}$ for $Fe_{62}Pd_{30}Ni_8$ (8 at.% Ni) alloys. However, the magnetostriction of the $Fe_{70}Pd_{30}$ alloy without added Ni is ($\lambda_{\parallel}^{s} = 51 \times 10^{-6}$; $\lambda_{\perp}^{s} = -10 \times 10^{-6}$). It is obvious that doping $Fe_{70}Pd_{30}$ alloys with Ni can substantially improve the magnetostriction of the alloys at RT. The magnetostrictive strains of the $Fe_{68}Pd_{30}Ni_2$ (2 at.% Ni) alloys ($\lambda_{\parallel}^{s} = 88 \times 10^{-6}$, $\lambda_{\perp}^{s} = -26 \times 10^{-6}$) were higher than those of the $Fe_{62}Pd_{30}Ni_8$ (8 at.% Ni) alloys ($\lambda_{\parallel}^{s} = 57 \times 10^{-6}$, $\lambda_{\perp}^{s} = -15 \times 10^{-6}$). The magnetostriction investigation indicates that at RT (300 K), the magnetostrictive strain decreases with increases in Ni content when the $Fe_{70-x}Pd_{30}Ni_x$ alloys are strain-forged to gain a ~38% reduction in thickness, annealed for recrystallization at 1100 °C for 8 h, and quenched in ice brine.

For alloys strain-forged to gain a ~38% reduction in thickness, recrystallization annealed at 1100 °C for 8 h and ST, the most important result of the high temperature (500 °C/100 h) aged $Fe_{70-x}Pd_{30}Ni_x$ (x = 2, 4, 6, 8 at.% Ni) alloys is shown in Fig. 12. The optimal magnetostrictive strains $\lambda_{\parallel}^{s}$ and $\lambda_{\perp}^{s}$ are plotted as a function of applied field (H) at RT (300 K) for the various Ni-content samples, indicating the following: $\lambda_{\parallel}^{s} = 16 \times 10^{-6}$, $\lambda_{\perp}^{s} = -4 \times 10^{-6}$ for $Fe_{68}Pd_{30}Ni_2$ (2 at.% Ni) alloys; $\lambda_{\parallel}^{s} = 22 \times 10^{-6}$, $\lambda_{\perp}^{s} = -7 \times 10^{-6}$ for $Fe_{66}Pd_{30}Ni_4$ alloys; $\lambda_{\parallel}^{s} = 56 \times 10^{-6}$, $\lambda_{\perp}^{s} = -12 \times 10^{-6}$ for $Fe_{64}Pd_{30}Ni_6$ alloys; and $\lambda_{\parallel}^{s} = 57 \times 10^{-6}$, $\lambda_{\perp}^{s} = -16 \times 10^{-6}$ for the $Fe_{62}Pd_{30}Ni_8$ (8 at.% Ni) alloys, respectively. The magnetostrictive strains of the $Fe_{70-x}Pd_{30}Ni_x$ (x = 2, 4 at.% Ni) alloys after aging at 500 °C for 100 h with a decrease in magnetostriction and magnetostrictive susceptibility ($\Delta\lambda_{\parallel}^{s}/\Delta H$) are shown in Fig. 12. The SEM and XRD analysis of the corresponding two aged alloys revealed that the decomposition of the $L1_0$+$L1_m$ twin phase into stoichiometric $L1_0$+$L1_m$+α_{bct} structures as well as the appearance of the XRD α_{bct} peak, as shown in Figs. 2(a)-(b) and Figs. 7(a)-(b). However, the magnetostrictive strains of the $Fe_{70-x}Pd_{30}Ni_x$ (x = 6, 8 at.% Ni) alloys after aging at 500 °C for 100 h maintained a high magnetostriction and magnetostrictive susceptibility ($\Delta\lambda_{\parallel}^{s}/\Delta H$), as shown in Fig. 12. The XRD analysis also revealed that these high Ni-content alloys, after 500 °C/100 h aging treatment, had a complete absence of the α_{bct} phase, and the decomposition of $L1_0$+$L1_m$ twin phase into stoichiometric $L1_0$+$L1_m$+α_{bct} structures also disappeared in the latter two aged samples, as shown in Figs. 7(c)-(d) and Figs. 2(c)-(d). The magnetic property demonstrates that the $Fe_{64}Pd_{30}Ni_6$ and $Fe_{62}Pd_{30}Ni_8$ alloys are suitable for application in a high temperature (T > 500 °C) and high frequency environment.

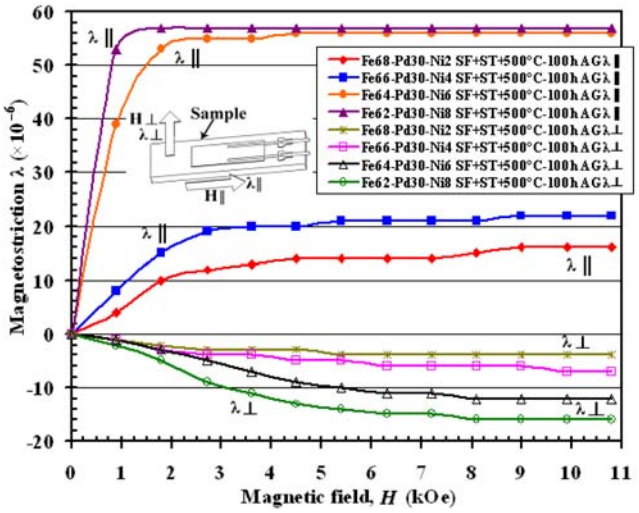

Fig. 12. (Color online) The linear magnetostriction (×10^{-6}) at RT (300 K) in parallel ($\lambda_{\parallel}$) and normal ($\lambda_{\perp}$) applied field (H (kOe)) to sample's longitude of the $Fe_{70-x}Pd_{30}Ni_x$ (x = 2, 4, 6, 8 at.% Ni) alloys strain-forged (SF) to gain a ~38% reduction in thickness and recrystallization annealed at 1100 °C for 8 h and ST, quenched in ice brine, and then aged at 500 °C for 100 h.

4. Conclusions

Magnetostriction measurements indicate that the $Fe_{70-x}Pd_{30}Ni_x$ (x = 2, 4, 6, 8 at.% Ni) alloys with greater Ni addition have decreased magnetostriction at room temperature (RT).

A higher Ni addition in the $Fe_{70-x}Pd_{30}Ni_x$ (x = 6, 8 at.% Ni) alloys increases magnetostriction and magnetostrictive susceptibility ($\Delta\lambda_{\parallel}^{s}/\Delta H$) after the alloys are strain-forged, ST, and aged at 500 °C for 100 h. The reason is that the decomposition of the $L1_0$+$L1_m$ twin phases into the stoichiometric $L1_0$+$L1_m$+α_{bct} structures is suppressed after the 500 °C/100 h aging treatment; therefore, the high Ni-content $Fe_{70-x}Pd_{30}Ni_x$ (x = 6, 8 at.% Ni) alloys are suitable for application in high temperature (T > 500 °C) and high frequency environments.

Low Ni-content $Fe_{70-x}Pd_{30}Ni_x$ (x = 2, 4 at.% Ni) alloys strain-forged, ST, and aged at 500 °C for 100 h undergo decomposition of the $L1_0$+$L1_m$ twin phases into the stoichiometric $L1_0$+$L1_m$+α_{bct} structures, which lead to a decrease of magnetostriction, as confirmed by SEM, x-ray diffraction and a magnetostrictive-meter setup, all of which showed consistent results.

After strain-forging, ST, and aging at 500 °C for 100 h, high Ni-content $Fe_{64}Pd_{30}Ni_6$ (6 at.% Ni) alloys possess a higher saturation magnetization (M_s), with a higher magneto-crystalline anisotropy energy constant (K_u) and lower coercivity than those of the low Ni-content $Fe_{66}Pd_{30}Ni_4$ (4 at.% Ni) alloys.

References

[1] P. K. Kumar and D. C. Lagoudas, Acta Mater. **58**, 1618 (2010).
[2] Y. Xin, Y. Li, and Zongde Liu, Scripta Mater. **63**, 35 (2010).
[3] Y. Li, Y. Xin, L. Chai, Y. Mad, and H. Xu, Acta Mater. **58**, 3655 (2010).
[4] J. Cui, T. W. Shield, and R. D. James, Acta Mater. **52**, 35 (2004).
[5] Y. C. Lin, C. F. Lin, J. B. Yang, and H. T. Lee, J. Appl. Phys. **109**, A912 (2011).
[6] J. G. Speer and D. V. Edmonds, Acta Metal. Mater. **36**, 1015 (1988).
[7] F. Appel, P. A. Beaven, and R. Wagner, Acta Metal. Mater. **41**, 1721 (1993).
[8] J. W. Christian, The Theory of Transformations in Metals and Alloys, Pergamon Press, Oxford (1965).
[9] K. C. Atli, I. Karaman, R. D. Noebe, and H. J. Maier, Scripta Mater. **64**, 315 (2011).
[10] C. F. Lin and J. B. Yang, IEEE Trans. Magn. **45**, 2499 (2009).